energy&fuels

pubs.acs.org/EF

Communication

Relationship between the Proton Conductive Performance and Water Uptake Ratio on a Filler-Filled Polymer Electrolyte Membrane

Takaaki Saito, Tomohiro Nohara,* Keisuke Tabata, Haruki Nakazaki, Tsutomu Makino, Yoshimasa Matsuo, Kei Sato, Colette Abadie, and Akito Masuhara*

Cite This: *Energy Fuels* 2022, 36, 13924−13929

Read Online

ACCESS | Metrics & More | Article Recommendations | Supporting Information

ABSTRACT: Polymer electrolyte fuel cells are attracting attention as clean, highly efficient power generation devices that can solve problems such as energy resource depletion, global warming, and environmental pollution. In this research, we have fabricated proton conductive filler-filled membranes, employing polymer-coated cellulose nanocrystals and different binder resins. Moreover, we have demonstrated the relationship between proton conductivity and water uptake of binder resins. It was clarified that the fabricated membrane with a high water uptake ratio showed excellent proton conduction performance under high humidity at low temperatures with a low activation energy for proton conduction. The substantiation of the compatibility relationship between water absorption and efficacy of proton conduction can contribute to the design and fabrication of a new binder resin synthesis model and contributes to the knowledge of the polymer skeleton structure for the improvement of the proton conductive performance of polymer electrolyte membranes.

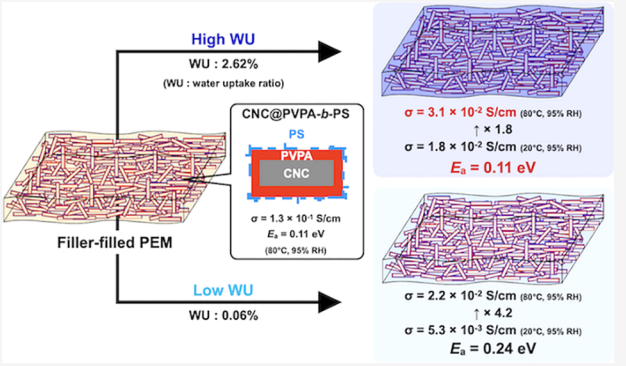

INTRODUCTION

Mixed matrix membranes (MMMs)[1] are hybrid membranes consisting of two or more components, such as inorganic/organic particles, polymers, and matrix resins. By mixing two or more components, it is possible to impart new properties that cannot be achieved by one material alone. MMMs have a wide range of applications, including gas separation membranes,[1,2] separators for electronic components,[3,4] and biomaterials. As such, much research has been conducted on these membranes. In recent years, MMMs, of which each component consists of a single domain of nano- or molecular order, have been developed to manufacture more precise devices and higher performance materials. However, it is difficult to achieve uniform mixing of different components in a microspace, resulting in interfacial defects and a significant decrease in performance.[5] Attempts have been made to increase performance using liquid fillers to fill in the interfacial defects.[6,7] However, it has been challenging to immobilize the liquid components within the polymer matrix as a result of the leaching of the liquid under differential pressure.[8−13] Nevertheless, there have been reports of the successful fabrication of membranes with few defects through surface modification of nanoparticles using grafting coupling agents and forming strong chemical bonds by coupling reactions between nanoparticle surfaces and the polymer matrix.[14] To suppress the performance degradation caused by the collapse of conduction channels as a result of interfacial defects, such as gas separation and electron/proton conductivity, it is necessary to fabricate MMMs without defective sites.[15−18]

Previously, we successfully fabricated polymer electrolyte membranes (PEMs) with high proton conductivity by mixing functionalized nanofillers. Nanoparticle surfaces were precisely coated with polymers that were highly compatible with matrix materials via reversible addition−fragmentation chain transfer (RAFT) polymerization with particles (PwP).[19−26] Specifically, cellulose nanocrystals (CNCs), known for their high aspect ratio and strength,[27] were used as the core nanoparticles. A copolymer of poly(vinylphosphonic acid) (PVPA) and polystyrene (PS) (PVPA-*b*-PS) was used as the shell polymer. The obtained functionalized nanoparticles, namely, CNC@PVPA-*b*-PS, were blended with polycarbonate (PC), a flexible and oxidation-resistant matrix resin. The membranes (CNC@PVPA-*b*-PS/PC) were fabricated using the doctor-blade method and then heat-pressed above the glass transition temperatures of their constituent polymers. The prepared PEM

Received: July 28, 2022
Revised: October 23, 2022
Published: October 26, 2022

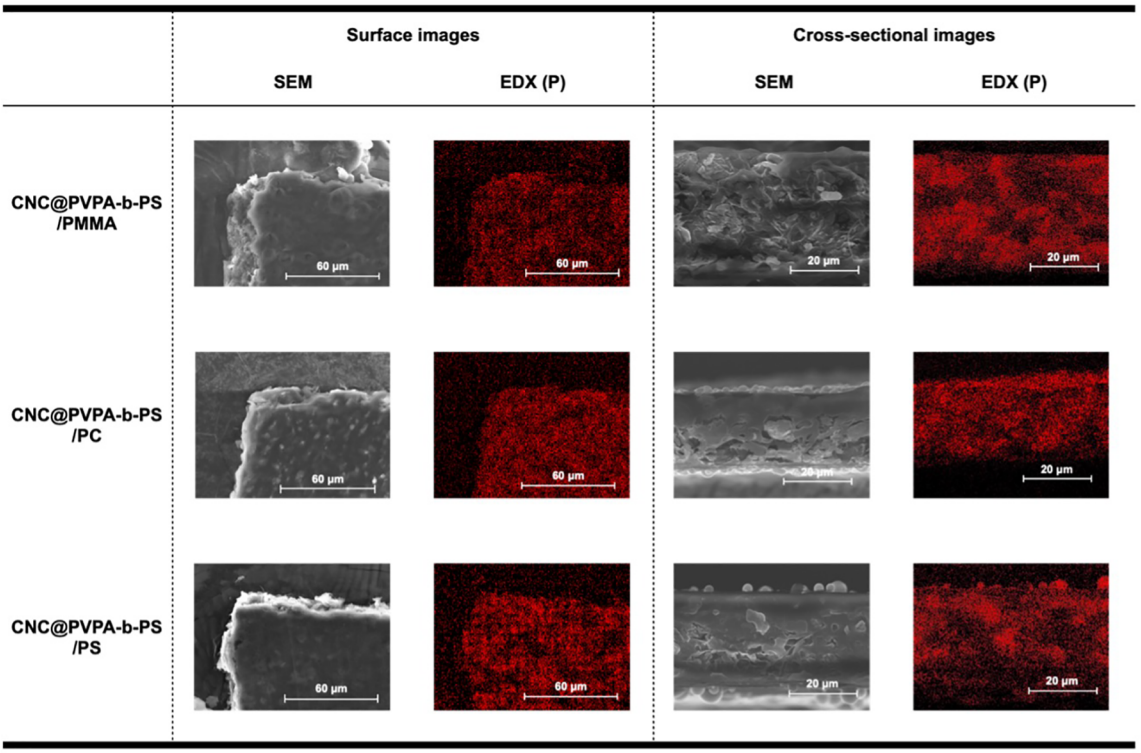

Figure 1. Surface and cross-sectional SEM images and EDX mapping of CNC@PVPA-*b*-PS/PMMA, CNC@PVPA-*b*-PS/PC, and CNC@PVPA-*b*-PS/PS.

was tested by inserting it into a single cell and examining its power generation characteristics. It was confirmed that direct current (DC) power was generated at room temperature under atmospheric conditions, indicating that the PEM was of a level that could be put to practical use. In contrast to existing PEM, such as Nafion,[28−30] which as a result of having superstrong acidity ($pK_a \sim -6$) by perfluorinated sulfonyl acid needs to use platinum for the catalyst and treat the acid durability around the system, the fabricated membranes have low acidity ($pK_a \sim 2.5$) and, thus, have the potential to generate electricity using catalysts other than platinum.[22] However, their proton conductivity was still about 1 order of magnitude lower than that of Nafion. To further improve proton conductivity, we focused on the water uptake ratios of the matrix resins. At low temperatures (below 100 °C), proton conductivity is correlated with the amount of water, which is the source of protons. We found that the higher the relative humidity, the higher the proton conductivity. Therefore, we expect that, under the same relative humidity, if we use material with higher water uptake for the matrix resin, the water content in the membrane should be higher, resulting in greater proton conductivity across the membrane.[31]

In this paper, we selected materials for the binder resin based on several criteria: variation in water uptake rates, the ability to use fabrication methods consistent with our previous experiments, general purpose, durability against redox reactions, and insolubility in hot water, as a result of the general operating environment of polymer electrolyte fuel cells (PEFCs)[32−36] having temperatures over 50 °C under wet conditions. Three binder resins, poly(methyl methacrylate) (PMMA), PC, and PS, were selected on the basis of these criteria and used to fabricate each membrane (CNC@PVPA-*b*-PS/PMMA, CNC@PVPA-*b*-PS/PC, and CNC@PVPA-*b*-PS/PS). The water uptake ratios of PMMA, PC, and PS are 2.62, 0.54, and 0.06%, respectively.[37] The effect of water absorption on proton conduction was investigated.

EXPERIMENTAL SECTION

The functionalized filler (CNC@PVPA-*b*-PS) was synthesized using the same fabrication methods used in previous experiments.[22] Obtained CNC@PVPA-*b*-PS (0.50 g) was dispersed in haloalkane, a highly polar solvent [10:1 mixture of dichloromethane (FUJIFILM Wako Pure Chemical Corporation)/1,2-dichloroethane (FUJIFILM Wako Pure Chemical Corporation)], used to dissolve the binder resins. Simultaneously, each binder resin was dissolved in the same mixture to make the resin solution.

Herein, the binder resins used in this paper are described. PMMA (0.50 g, FUJIFILM Wako Pure Chemical Corporation) is one of the most affordable resins with a high degree of weatherability, but it has low heat resistance (up to 95 °C) and is vulnerable to strong alkalis. The water uptake ratio of a membrane consisting only of PMMA is 2.62%, which is the highest water uptake ratio of all binder resins used in this paper. PC (Panlite K-1300Y, 0.50 g, TEIJIN) is one of the best candidates for PEFC membrane binders because of its high moldability and high stability against weathering and temperature.[38] The water uptake ratio of a membrane consisting only of PC is 0.54%. Finally, PS ($M_w \sim 280\,000$, 0.50 g, Sigma-Aldrich), the same polymer as the outermost layer of CNC@PVPA-*b*-PS, is compatible with highly polar solvents. Therefore, CNC@PVPA-*b*-PS can evenly disperse throughout the membrane. The water uptake ratio of a membrane consisting only of PS is 0.06%, which is one of the lowest water uptake ratios of the general resins.[39]

The filler dispersion and the resin solution were mixed thoroughly using ultrasonication, kneading, and deforming techniques. The resulting slurries of filler and resins were cast and thinned using the doctor-blade method on the poly(ethylene terephthalate) (PET) film in a climate-controlled glovebox [under 25 °C and 25% relative humidity (RH)]. The coated membrane was then left at room temperature to allow the solvents to evaporate. After drying, the PET

https://doi.org/10.1021/acs.energyfuels.2c02527
Energy Fuels 2022, 36, 13924−13929

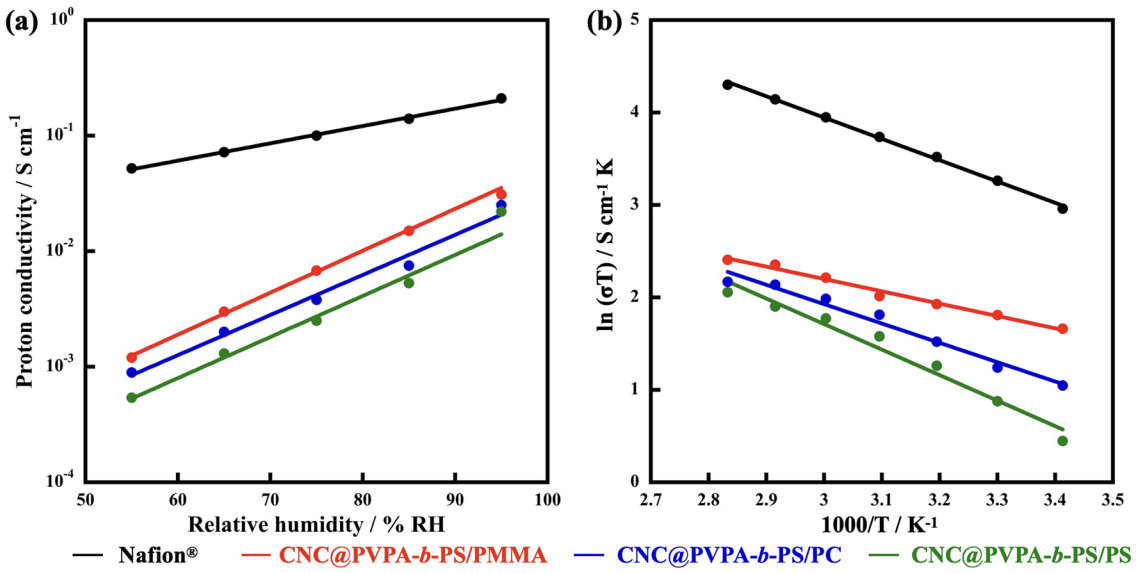

Figure 2. (a) Relative humidity−proton conductivity plots under different RH (55−95%) at 80 °C and (b) Arrhenius plots under 95% RH at different temperatures (20−80 °C) for Nafion (black line), CNC@PVPA-*b*-PS/PMMA membrane (red line), CNC@PVPA-*b*-PS/PC (orange line), and CNC@PVPA-*b*-PS/PS (green line).

Table 1. Summary of Proton Conductivities and E_a of the Nafion Membrane, CNC@PVPA-*b*-PS/PMMA, CNC@PVPA-*b*-PS/PC, and CNC@PVPA-*b*-PS/PS (Top) under 95% RH at Different Temperatures (20−80°C) and (Bottom) under Different RH (55−95% RH) at 80 °C

80 °C(S/cm)	95% RH	85% RH	75% RH	65% RH	55% RH
Nafion (WU = 23.7%)	2.1×10^{-1}	1.4×10^{-1}	1.0×10^{-1}	7.2×10^{-2}	5.2×10^{-2}
CNC@PVPA-*b*-PS/PMMA(WU = 30.0%)	3.5×10^{-2}	1.5×10^{-2}	6.8×10^{-3}	3.0×10^{-3}	1.2×10^{-3}
CNC@PVPA-*b*-PS/PC(WU = 25.1%)	2.5×10^{-2}	7.5×10^{-3}	3.8×10^{-3}	2.0×10^{-3}	8.9×10^{-4}
CNC@PVPA-*b*-PS/PS(WU = 17.6%)	1.6×10^{-2}	5.3×10^{-3}	2.5×10^{-3}	1.3×10^{-3}	5.4×10^{-4}

95% RH(S/cm)	80 °C	70 °C	60 °C	50 °C	40 °C	30 °C	20 °C	E_a (eV)
Nafion (WU = 23.7%)	2.1×10^{-1}	1.8×10^{-1}	1.6×10^{-1}	1.3×10^{-1}	1.1×10^{-1}	8.6×10^{-2}	6.6×10^{-2}	0.19
CNC@PVPA-*b*-PS/PMMA(WU = 30.0%)	3.1×10^{-2}	3.1×10^{-2}	2.8×10^{-2}	2.3×10^{-2}	2.2×10^{-2}	2.0×10^{-2}	1.8×10^{-2}	0.11
CNC@PVPA-*b*-PS/PC(WU = 25.1%)	2.5×10^{-2}	2.5×10^{-2}	2.2×10^{-2}	1.9×10^{-2}	1.5×10^{-2}	1.1×10^{-2}	9.7×10^{-3}	0.18
CNC@PVPA-*b*-PS/PS(WU = 17.6%)	2.2×10^{-2}	2.0×10^{-2}	1.8×10^{-2}	1.5×10^{-2}	1.1×10^{-2}	7.9×10^{-3}	5.3×10^{-3}	0.24

film was peeled off to obtain the filler-filled membranes. To closely connect the proton conductive pathways of the filler surfaces, the obtained filler-filled membranes were hot-pressed with 1000 kg of pressure for 5 min. The glass transition temperatures of PMMA, PC, and PS are 105, 150, and 100 °C, respectively; therefore, the temperature was set to 160 °C to unify the hot press temperature and exceed the glass transition point.

Fourier transform infrared (FTIR) spectra and thermogravimetric analysis (TGA) curves are shown in Figures S1 and S2 of the Supporting Information, respectively.

Water uptake ratios of the membranes [WU (%)] were calculated using eq 1

$$\mathrm{WU} = \frac{W_{\mathrm{wet}} - W_{\mathrm{dry}}}{W_{\mathrm{dry}}} \times 100 \tag{1}$$

where the wet membrane [W_{wet} (g)] was immersed in 20 °C ultrapure water for 1 day and the dry membrane [W_{dry} (g)] was dried in the dry oven at 80 °C for 1 day.[40,41]

The proton conductivities were measured using the alternating current (AC) impedance method with the impedance analyzer (IM 3570, HIOKI E.E. Corp., frequency of 4.6−4.6 × 10^6 Hz, four-terminal method). The measuring cells, set up in the same manner as in our previous paper, were placed in an environment control machine (bench-top-type temperature and humidity chamber, SH-222, ESPEC Corp.) and was measured under various relative humidities (55−95% RH) at 80 °C and under 95% RH at temperatures ranging from 20 to 80 °C. When proton conductivity is measured, these cells are observed in the measurement environment during *in situ* measurement with the AC impedance method until the time when the water absorption of these membranes is saturated; i.e., the proton conductivity values are stabilized. From the Cole−Cole plots (Figures S3 and S4 of the Supporting Information), the inflection points were regarded as the bulk resistance of each sample. Using the values of bulk impedance [R_s (Ω)], distance between gold wires [d (cm)], and proton-conducting surface area [S (cm^2)], which was calculated by membrane thickness × width, the proton conductivities [σ (S/cm)] can be calculated using eq 2.

$$\sigma = \frac{1}{R_s}\frac{d}{S} \tag{2}$$

The activation energies [E_a (eV)] were calculated using the Arrhenius equation (eq 3)

$$\sigma T = \sigma_0 \exp\left(-\frac{E_a}{kT}\right) \tag{3}$$

where the proton conductivity is [σ (S/cm)], the absolute temperature is [T (K)], the pre-exponential factor is [σ_0 (S K^{-1} cm^{-1})], and the Boltzmann constant is [k (8.6171 × 10^{-5} eV/K)].

https://doi.org/10.1021/acs.energyfuels.2c02527
Energy Fuels 2022, 36, 13924−13929

RESULTS AND DISCUSSION

Figure 1 shows the scanning electron microscopy (SEM) and energy-dispersive X-ray (EDX) mapping distribution targeted for phosphorus from the aspect of the surface and cross section for CNC@PVPA-*b*-PS/PMMA, CNC@PVPA-*b*-PS/PC, and CNC@PVPA-*b*-PS/PS. The surface EDX mappings of filler-filled membranes confirm that the EDX signal derived from the phosphorus atom was localized on the membrane surface and spread uniformly over the entire membrane with no aggregations. Additionally, the cross-sectional EDX mappings confirm that the EDX signal derived from the phosphorus atom was also localized and spread across the membrane area. Therefore, the filler was filled into these binder resins in the same way. In our previous research,[22] the compatibility between binder resin and the outermost layer of functionalized filler critically affected the dispersity in the filler-filled membranes. However, in this research, there is no relationship between the water uptake ratio of binder resins and dispersity in filler-filled membranes.

Figure 2a shows the function of the relative humidity (55−95% RH)−proton conductivity at 80 °C for Nafion, CNC@PVPA-*b*-PS/PMMA, CNC@PVPA-*b*-PS/PC, and CNC@PVPA-*b*-PS/PS, and Table 1 summarizes the water uptake ratio, proton conductivities, and activation energies for each sample. As a result of the functionalized filler, the water uptake ratios drastically increased, such as PMMA to CNC@PVPA-*b*-PS/PMMA, 2.62−30.0%; PC to CNC@PVPA-*b*-PS/PC, 0.54−25.1%; and PS to CNC@PVPA-*b*-PS/PS, 0.06−17.6%, respectively.

Comparatively, in Nafion, the proton conductivity achieved more than 5×10^{-2} S/cm in all measured ranges of relative humidity and exceeded 1×10^{-1} S/cm over 75% RH at 80 °C. Nafion shows excellent performance because it can keep high proton conductivity, even if it is in the low-humidity condition.

On the other hand, each filler-filled membrane showed 1 order of proton conductivity less than Nafion. Like Nafion, the proton conductivity exponentially increased with relative humidity. In comparison to each other, it was confirmed that the proton conductivity was critically related to the water uptake ratio of binder resins. Protons have higher molar conductivity than sodium cations, chloride anions, or any other ions in water. This is because protons can diffuse not only through the self-diffusion mechanism (vehicle mechanism) but also by hopping through the hydrogen bonds formed between water molecules (Grötthuss mechanism).[42,43] In other words, because the high water uptake filler-filled membranes contain more water molecules than the low water uptake filler-filled membranes in the same environment, the proton conductivity increases as a result of the activation of proton diffusion by both the vehicle mechanism and Grötthuss mechanism. As such, the proton conductivity of filler-filled membranes is correlated with their water uptake ratio, with PMMA having the highest proton conductivity, followed by PC, and PS having the lowest proton conductivity. Additionally, the filler-filled membranes had a steeper slope than Nafion. This suggests that the fillers dramatically increase the water uptake ratio in the membranes. These results demonstrate that the water uptake of the filler-filled membrane can be controlled by changing the filler content ratio.

Figure 2b shows the Arrhenius plots under 95% RH at different temperatures (20−80 °C) for Nafion, CNC@PVPA-*b*-PS/PMMA, CNC@PVPA-*b*-PS/PC, and CNC@PVPA-*b*-PS/PS. The proton conductivity increased with the temperature because of the motility of activated water molecules and protons by heat. In general, the lower the activation energy, the faster the ion conduction rate, which can be used to estimate the ion conduction mechanisms. As mentioned above, there are two types of conduction mechanisms for protons, the vehicle mechanism and the Grötthuss mechanism, which have the activation energy over 0.4 eV and the activation energy below 0.4 eV, respectively. However, these two conduction mechanisms can occur simultaneously. The activation energy is high when the vehicle mechanism is dominant and low when the Grötthuss mechanism is dominant. Nafion achieved proton conductivity over 6×10^{-2} S/cm in all measured ranges of the temperature and exceeded 1×10^{-1} S/cm from 40 °C under 95% RH with E_a = 0.22 eV. Therefore, from panels a and b of Figure 2, the Nafion membrane shows excellent proton conductivity performance in low-temperature (<100 °C) environments.

In filler-filled membranes, proton conductivity increased with the water uptake ratio, demonstrating the relationship between relative humidity and proton conductivity. At temperatures over 40 °C under 95% RH, all proton conductivities achieved 10^{-2} S/cm, which is a good level for practical applications. The activation energies of these samples were in descending order against the water uptake ratio. This is likely because the binder, which has a high water uptake ratio like PMMA, can absorb much water, even if it is exposed to low humidity in a low-temperature environment. Therefore, the proton conductivity performance of the high water uptake ratio membrane was almost completely dominated by the Grötthuss mechanism in low-temperature environments. Because the water uptake ratio does not change significantly as the temperature rises, there is no significant improvement in proton conductivity associated with the temperature increase. Furthermore, stable proton conductivity can be shown from low temperatures (20 °C) to high temperatures (80 °C). On the other hand, the binder, which has a low water uptake ratio like PS, cannot absorb enough water under low temperatures. As the temperature is increased, the water uptake ratio gradually ticks up, resulting in a greater increase in proton conductivity than in high water uptake ratio binders. Thus, we have shown that protons mainly conduct via the vehicle mechanism at lower temperatures, but the Grötthuss mechanism becomes the dominant mechanism as the temperature rises. Therefore, the activation energy of the low water uptake ratio binders was higher than that of high water uptake ratio binders. However, the activation energy does not continue to increase, which suggests that it has a limit. As shown in Figure S5 of the Supporting Information, the clear change in activation energy can be observed in a low water uptake ratio binder at 50 °C. Taking this into consideration, practical applications should use a binder with a high water uptake ratio membrane that can provide stable proton conductivity over a wide temperature range, provided that there is no swelling and collapsing of the membrane shape.

CONCLUSION

In summary, we have successfully fabricated the filler-filled membrane composed of functionalized filler of CNC@PVPA-*b*-PS and three binder resins (PMMA, PC, and PS), which have different water uptake ratios, and revealed the relationship between the water uptake ratio and the proton conductivity performance. The proton conductivity of filler-filled mem-

https://doi.org/10.1021/acs.energyfuels.2c02527
Energy Fuels 2022, 36, 13924−13929

branes is strongly correlated with the water uptake ratio, where the higher the water uptake ratio, the higher the proton conductivity in all environmental ranges studied in this paper (under 55−95% RH at 80 °C and under 95% RH at 20−80 °C). The activation energy of the filler-filled membrane was also closely related to the water uptake ratio, where the higher the water uptake ratio, the lower the activation energy for conditions under 95% RH at 20−80 °C. These results were attributed to the proton transport mechanism mediated by water molecules. For a membrane with a high water uptake ratio, water is sufficiently absorbed into the membrane, even in low-temperature and low-humidity conditions. Protons are conducted via the Grötthuss mechanism, which conducts through water molecules, resulting in low activation energy and high proton conductivity. Conversely, for membranes with low water uptake ratios, the ability to absorb water into the membrane is extremely small in low-temperature and low-humidity conditions. Therefore, water molecules move by themselves as oxonium ions, which are conducted via the vehicle mechanism, resulting in low proton conductivity and high activation energy. This knowledge serves as an important design guideline for the selection of binders in filler-filled membranes. As long as swelling or membrane collapse as a result of excessive water absorption does not occur, selecting a binder with as high of a water uptake ratio as possible will result in consistently high proton conductivity and low activation energy over a wide range of temperature and humidity environments.

■ ASSOCIATED CONTENT

Supporting Information

The Supporting Information is available free of charge at https://pubs.acs.org/doi/10.1021/acs.energyfuels.2c02527.

Results of FTIR (Figure S1), TGA curves (Figure S2), Cole−Cole plots (Figures S3 and S4), Arrhenius plots, which were split by a vertical black dotted line at 50 °C (Figure S5), plot of WU and proton conductivity (Figure S6), and comparison of the proton conductive performance to others (Table S1) (PDF)

■ AUTHOR INFORMATION

Corresponding Authors

Tomohiro Nohara − *Graduate School of Science and Engineering, Yamagata University, Yonezawa, Yamagata 992-8510, Japan;* orcid.org/0000-0003-3299-0021; Phone: +81-238-26-3891; Email: tyk95026@st.yamagata-u.ac.jp

Akito Masuhara − *Graduate School of Science and Engineering, Yamagata University, Yonezawa, Yamagata 992-8510, Japan; Frontier Center for Organic Materials (FROM), Yamagata University, Yonezawa, Yamagata 992-8510, Japan;* orcid.org/0000-0001-7108-959X; Phone: +81-238-26-3891; Email: masuhara@yz.yamagata-u.ac.jp

Authors

Takaaki Saito − *Graduate School of Science and Engineering, Yamagata University, Yonezawa, Yamagata 992-8510, Japan;* orcid.org/0000-0003-1746-5667

Keisuke Tabata − *Graduate School of Science and Engineering, Yamagata University, Yonezawa, Yamagata 992-8510, Japan*

Haruki Nakazaki − *Graduate School of Science and Engineering, Yamagata University, Yonezawa, Yamagata 992-8510, Japan*

Tsutomu Makino − *Graduate School of Science and Engineering, Yamagata University, Yonezawa, Yamagata 992-8510, Japan*

Yoshimasa Matsuo − *Faculty of Engineering, Yamagata University, Yonezawa, Yamagata 992-8510, Japan*

Kei Sato − *Faculty of Engineering, Yamagata University, Yonezawa, Yamagata 992-8510, Japan*

Colette Abadie − *Department of Physics, University of Vermont, Burlington, Vermont 05405, United States*

Complete contact information is available at: https://pubs.acs.org/10.1021/acs.energyfuels.2c02527

Author Contributions

Corresponding authors Tomohiro Nohara and Akito Masuhara conceived and planned the presented idea, acquired the funds, and supervised the paper. Takaaki Saito and Colette Abadie carried out the experiment, analyzed the data, and prepared the manuscript. Keisuke Tabata, Tsutomu Makino, and Yoshimasa Matsuo analyzed the filler properties. Haruki Nakazaki and Kei Sato carried out the membrane electrode preparation. Whole experimental results were discussed by all of the authors.

Notes

The authors declare no competing financial interest.

■ REFERENCES

(1) Wong, K. K.; Jawad, Z. A. A review and future prospect of polymer blend mixed matrix membrane for CO_2 separation. *J. Polym. Res.* **2019**, *26* (12), 289.

(2) Kamble, A. R.; Patel, C. M.; Murthy, Z. V. P. A review on the recent advances in mixed matrix membranes for gas separation processes. *Renewable Sustainable Energy Rev.* **2021**, *145*, 111062.

(3) Bakangura, E.; Wu, L.; Ge, L.; Yang, Z.; Xu, T. Mixed matrix proton exchange membranes for fuel cells: State of the art and perspectives. *Prog. Polym. Sci.* **2016**, *57*, 103−152.

(4) Mohanapriya, S.; Bhat, S. D.; Sahu, A. K.; Pitchumani, S.; Sridhar, P.; Shukla, A. K. A new mixed-matrix membrane for DMFCs. *Energy Environ. Sci.* **2009**, *2* (11), 1210−1216.

(5) Sadeghi, N.; Bakhtiari, O. Modification of Mixed Matrix Membranes' Famous Permeability Prediction Models by Considering the Formed Voids around Nonporous Fillers. *Iran. J. Chem. Eng.* **2020**, *17* (3), 53−73.

(6) Bakhtiari, O.; Sadeghi, N. The Formed Voids around the Filler Particles Impact on the Mixed Matrix Membranes' Gas Permeabilities. *Int. J. Chem. Eng. Appl.* **2014**, *5*, 198−203.

(7) Mahajan, R.; Koros, W. J. Mixed matrix membrane materials with glassy polymers. Part 1. *Polym. Eng. Sci.* **2002**, *42* (7), 1420−1431.

(8) Lau, C. H.; Konstas, K.; Doherty, C. M.; Kanehashi, S.; Ozcelik, B.; Kentish, S. E.; Hill, A. J.; Hill, M. R. Tailoring Physical Aging in Super Glassy Polymers with Functionalized Porous Aromatic Frameworks for CO_2 Capture. *Chem. Mater.* **2015**, *27* (13), 4756−4762.

(9) Lau, C. H.; Mulet, X.; Konstas, K.; Doherty, C. M.; Sani, M.-A.; Separovic, F.; Hill, M. R.; Wood, C. D. Hypercrosslinked Additives for Ageless Gas-Separation Membranes. *Angew. Chem., Int. Ed.* **2016**, *55* (6), 1998−2001.

(10) Lau, C. H.; Konstas, K.; Thornton, A. W.; Liu, A. C. Y.; Mudie, S.; Kennedy, D. F.; Howard, S. C.; Hill, A. J.; Hill, M. R. Gas-Separation Membranes Loaded with Porous Aromatic Frameworks that Improve with Age. *Angew. Chem., Int. Ed.* **2015**, *54* (9), 2669−2673.

(11) Lau, C. H.; Nguyen, P. T.; Hill, M. R.; Thornton, A. W.; Konstas, K.; Doherty, C. M.; Mulder, R. J.; Bourgeois, L.; Liu, A. C.

Y.; Sprouster, D. J.; Sullivan, J. P.; Bastow, T. J.; Hill, A. J.; Gin, D. L.; Noble, R. D. Ending Aging in Super Glassy Polymer Membranes. *Angew. Chem., Int. Ed.* **2014**, *53* (21), 5322−5326.
(12) Kanehashi, S.; Gu, H.; Shindo, R.; Sato, S.; Miyakoshi, T.; Nagai, K. Gas permeation and separation properties of polyimide/ZSM-5 zeolite composite membranes containing liquid sulfolane. *J. Appl. Polym. Sci.* **2013**, *128* (6), 3814−3823.
(13) Shindo, R.; Kishida, M.; Sawa, H.; Kidesaki, T.; Sato, S.; Kanehashi, S.; Nagai, K. Characterization and gas permeation properties of polyimide/ZSM-5 zeolite composite membranes containing ionic liquid. *J. Membr. Sci.* **2014**, *454*, 330−338.
(14) Setiawan, W. K.; Chiang, K.-Y. Silica applied as mixed matrix membrane inorganic filler for gas separation: A review. *Sustainable Environ. Res.* **2019**, *29* (1), 32.
(15) Nagao, Y. Proton-Conductivity Enhancement in Polymer Thin Films. *Langmuir* **2017**, *33* (44), 12547−12558.
(16) Nagao, Y. Progress on highly proton-conductive polymer thin films with organized structure and molecularly oriented structure. *Sci. Technol. Adv. Mater.* **2020**, *21* (1), 79−91.
(17) Suwansoontorn, A.; Yamamoto, K.; Nagano, S.; Matsui, J.; Nagao, Y. Interfacial and Internal Proton Conduction of Weak-acid Functionalized Styrene-based Copolymer with Various Carboxylic Acid Concentrations. *Electrochemistry* **2021**, *89* (5), 401−408.
(18) Tsuksamoto, M.; Ebata, K.; Sakiyama, H.; Yamamoto, S.; Mitsuishi, M.; Miyashita, T.; Matsui, J. Biomimetic Polyelectrolytes Based on Polymer Nanosheet Films and Their Proton Conduction Mechanism. *Langmuir* **2019**, *35* (9), 3302−3307.
(19) Arita, T. Efficient Production of Block-copolymer-coated Ceramic Nanoparticles by Sequential Reversible Addition-Fragmentation Chain-transfer Polymerizations with Particles (SqRAFTwP). *Chem. Lett.* **2013**, *42* (8), 801−803.
(20) Arita, T.; Kanahara, M.; Motoyoshi, K.; Koike, K.; Higuchi, T.; Yabu, H. Localization of polymer-grafted maghemite nanoparticles in a hemisphere of Janus polymer particles prepared by a self-organized precipitation (SORP) method. *J. Mater. Chem. C* **2013**, *1* (2), 207−212.
(21) Koseki, K.; Arita, T.; Tabata, K.; Nohara, T.; Sato, R.; Nagano, S.; Masuhara, A. Effect of Surface Silanol Density on the Proton Conductivity of Polymer-Surface-Functionalized Silica Nanoparticles. *ACS Sustainable Chem. Eng.* **2021**, *9* (30), 10093−10099.
(22) Nohara, T.; Arita, T.; Tabata, K.; Saito, T.; Shimada, R.; Nakazaki, H.; Suzuki, Y.; Sato, R.; Masuhara, A. Novel Filler-Filled-Type Polymer Electrolyte Membrane for PEFC Employing Poly-(vinylphosphonic acid)-b-polystyrene-Coated Cellulose Nanocrystals as a Filler. *ACS Appl. Mater. Interfaces* **2022**, *14* (6), 8353−8360.
(23) Nohara, T.; Koseki, K.; Tabata, K.; Shimada, R.; Suzuki, Y.; Umemoto, K.; Takeda, M.; Sato, R.; Rodbuntum, S.; Arita, T.; Masuhara, A. Core Size-Dependent Proton Conductivity of Silica Filler-Functionalized Polymer Electrolyte Membrane. *ACS Sustainable Chem. Eng.* **2020**, *8* (39), 14674−14678.
(24) Shito, K.; Matsui, J.; Takahashi, Y.; Masuhara, A.; Arita, T. Proton Conductivity of Poly(acrylic acid)-b-Polystyrene-coated Silica Nanoparticles Synthesized by Reversible Addition-Fragmentation Chain Transfer Polymerization with Particles. *Chem. Lett.* **2018**, *47* (1), 9−12.
(25) Suzuki, Y.; Nohara, T.; Tabata, K.; Yamakado, R.; Shimada, R.; Nakazaki, H.; Saito, T.; Makino, T.; Arita, T.; Masuhara, A. Proton conductive polymeric ionic liquids block copolymer of poly-(vinylphosphonic acid)/1-propylimidazole-b-polystyrene for polymer electrolyte membrane fuel cell. *Jpn. J. Appl. Phys.* **2022**, *61* (SI), SD1034.
(26) Tabata, K.; Nohara, T.; Koseki, K.; Umemoto, K.; Sato, R.; Rodbuntum, S.; Suzuki, Y.; Shimada, R.; Asakura, S.; Arita, T.; Masuhara, A. Facile-controlling of the coating amount of poly(acrylic acid)-*b*-polystyrene coated on silica nanoparticles for polymer electrolyte membrane. *Jpn. J. Appl. Phys.* **2020**, *59* (SI), SIIH01.
(27) Sato, R.; Arita, T.; Shimada, R.; Nohara, T.; Tabata, K.; Koseki, K.; Umemoto, K.; Masuhara, A. Biocompatible composite of cellulose nanocrystal and hydroxyapatite with large mechanical strength. *Cellulose* **2021**, *28* (2), 871−879.
(28) Feng, K.; Tang, B.; Wu, P. Sulfonated graphene oxide-silica for highly selective Nafion-based proton exchange membranes. *J. Mater. Chem. A* **2014**, *2* (38), 16083−16092.
(29) Sahu, A. K.; Ketpang, K.; Shanmugam, S.; Kwon, O.; Lee, S.; Kim, H. Sulfonated Graphene-Nafion Composite Membranes for Polymer Electrolyte Fuel Cells Operating under Reduced Relative Humidity. *J. Phys. Chem. C* **2016**, *120* (29), 15855−15866.
(30) Tsipoaka, M.; Aziz, M. A.; Shanmugam, S. Degradation-Mitigating Composite Membrane That Exceeds a 1 W cm-2 Power Density of a Polymer Electrolyte Membrane Fuel Cell Operating Under Dry Conditions. *ACS Sustainable Chem. Eng.* **2021**, *9* (7), 2693−2704.
(31) Wang, F.; Wang, D.; Nagao, Y. OH- Conductive Properties and Water Uptake of Anion Exchange Thin Films. *ChemSusChem* **2021**, *14* (13), 2694−2697.
(32) Kang, D. W.; Kang, M.; Hong, C. S. Post-synthetic modification of porous materials: Superprotonic conductivities and membrane applications in fuel cells. *J. Mater. Chem. A* **2020**, *8* (16), 7474−7494.
(33) Santos, L. D.; Maréchal, M.; Guillermo, A.; Lyonnard, S.; Moldovan, S.; Ersen, O.; Sel, O.; Perrot, H.; Laberty-Robert, C. Proton Transport in Electrospun Hybrid Organic-Inorganic Membranes: An Illuminating Paradox. *Adv. Funct. Mater.* **2016**, *26* (4), 594−604.
(34) Steininger, H.; Schuster, M.; Kreuer, K. D.; Kaltbeitzel, A.; Bingöl, B.; Meyer, W. H.; Schauff, S.; Brunklaus, G.; Maier, J.; Spiess, H. W. Intermediate temperature proton conductors for PEM fuel cells based on phosphonic acid as protogenic group: A progress report. *Phys. Chem. Chem. Phys.* **2007**, *9* (15), 1764−1773.
(35) Titvinidze, G.; Kreuer, K.-D.; Schuster, M.; de Araujo, C. C.; Melchior, J. P.; Meyer, W. H. Proton Conducting Phase-Separated Multiblock Copolymers with Sulfonated Poly(phenylene sulfone) Blocks for Electrochemical Applications: Preparation, Morphology, Hydration Behavior, and Transport. *Adv. Funct. Mater.* **2012**, *22* (21), 4456−4470.
(36) Zhang, H.; Shen, P. K. Advances in the high performance polymer electrolyte membranes for fuel cells. *Chem. Soc. Rev.* **2012**, *41* (6), 2382−2394.
(37) Xi, G.; Xiao, M.; Wang, S.; Han, D.; Li, Y.; Meng, Y. Polymer-Based Solid Electrolytes: Material Selection, Design, and Application. *Adv. Funct. Mater.* **2021**, *31* (9), 2007598.
(38) Aguilar-Vega, M.; Paul, D. R. Gas transport properties of polycarbonates and polysulfones with aromatic substitutions on the bisphenol connector group. *J. Polym. Sci., Part B: Polym. Phys.* **1993**, *31* (11), 1599−1610.
(39) Puleo, A. C.; Muruganandam, N.; Paul, D. R. Gas sorption and transport in substituted polystyrenes. *J. Polym. Sci., Part B: Polym. Phys.* **1989**, *27* (11), 2385−2406.
(40) Albert, A.; Barnett, A. O.; Thomassen, M. S.; Schmidt, T. J.; Gubler, L. Radiation-Grafted Polymer Electrolyte Membranes for Water Electrolysis Cells: Evaluation of Key Membrane Properties. *ACS Appl. Mater. Interfaces* **2015**, *7* (40), 22203−22212.
(41) Ketpang, K.; Lee, K.; Shanmugam, S. Facile Synthesis of Porous Metal Oxide Nanotubes and Modified Nafion Composite Membranes for Polymer Electrolyte Fuel Cells Operated under Low Relative Humidity. *ACS Appl. Mater. Interfaces* **2014**, *6* (19), 16734−16744.
(42) Fan, P.; Liu, H.; Marosz, V.; Samuels, N. T.; Suib, S. L.; Sun, L.; Liao, L. High Performance Composite Polymer Electrolytes for Lithium-Ion Batteries. *Adv. Funct. Mater.* **2021**, *31* (23), 2101380.
(43) Zheng, Y.; Yao, Y.; Ou, J.; Li, M.; Luo, D.; Dou, H.; Li, Z.; Amine, K.; Yu, A.; Chen, Z. A review of composite solid-state electrolytes for lithium batteries: Fundamentals, key materials and advanced structures. *Chem. Soc. Rev.* **2020**, *49* (23), 8790−8839.

https://doi.org/10.1021/acs.energyfuels.2c02527
Energy Fuels 2022, 36, 13924−13929